

Aggregate pore and shape properties were more strongly correlated to soil organic carbon in large aggregates: Evidence from a long-term management-induced soil carbon gradient

Weijun Zhang^{a,b}, Lars J. Munkholm^a , Richard J. Heck^c, Christopher W. Watts^d ,
Johannes L. Jensen^{a,*}

^a Department of Agroecology, Aarhus University, AU-Viborg, Blichers Allé 20, DK-8830 Tjele, Denmark

^b Key Laboratory of Vegetation Restoration and Management of Degraded Ecosystems, Guangdong Provincial Key Laboratory of Applied Botany, South China Botanical Garden, Chinese Academy of Sciences, Guangzhou, China

^c School of Environmental Sciences, University of Guelph, 50 Stone Road E, Guelph, Ontario N1G2W1, Canada

^d Rothamsted Research, Harpenden, Hertfordshire AL5 2JQ, United Kingdom

ARTICLE INFO

Keywords:

Aggregates
Aggregate shape characteristics
Porosity
Soil management
X-ray CT

ABSTRACT

The interplay between soil structure and soil organic carbon (SOC) is complex and affects key soil functions. There is limited knowledge on how this relationship changes with the size of the structural unit studied. The objective of this study was to quantify the pore and shape characteristics of soil aggregates of varying sizes, and their relationships with SOC under different soil management regimes. Soils were sampled in March 2015 from the Highfield Ley-Arable Long-Term Experiment at Rothamsted Research. This experiment includes bare fallow, continuous arable rotation, ley-arable rotation, and grass treatments. A total of 24 aggregates from each treatment and size class (2–4, 4–8, and 8–16 mm) were subjected to X-ray micro-CT scanning at 40 µm voxel resolution. Results showed that permanent grass not only increased SOC accumulation, but also promoted pore connectivity of soil aggregates compared to bare fallow, regardless of aggregate size. Additionally, the pore and shape characteristics of larger aggregates (4–8 and 8–16 mm) were more sensitive to soil management compared to smaller aggregates (2–4 mm). The relationships between SOC and aggregate structural characteristics were strong for both 8–16 and 4–8 mm aggregates but weak for 2–4 mm aggregates. Furthermore, the responses of pore connectivity and sphericity to SOC increased with aggregate size. The results suggest that organic matter input plays an essential role in shaping aggregate structural characteristics and aggregate rearrangement (especially in larger aggregates).

1. Introduction

Soil structure can be understood as the arrangement of solids and pores with profound effects on soil functioning (Vogel et al., 2022). Soil structure is generally studied on intact soil cores “pore approach” and/or on isolated soil structural units known as aggregates “aggregate approach”, as outlined and discussed by Vogel et al. (2022). The aggregates are typically organized in a hierarchy of different sized aggregates (Yudina and Kuzyakov, 2019). Soil aggregates are formed by

complex biotic and abiotic interactions and occur at the µm to dm scale (Yudina and Kuzyakov, 2023). They play important roles in vital soil functions (storage and availability of carbon, nutrients and water, structural stability, water infiltration, habitat for soil microorganisms, soil fauna, and roots) as discussed by Yudina and Kuzyakov (2019; 2023). The interaction between soil organic carbon (SOC) and soil particles is crucial for the formation of aggregates (Bucka et al., 2019) and at the same time aggregates are of vital importance for SOC stabilization and storage (Six and Paustian, 2014). According to aggregate

Abbreviations: SOC, soil organic carbon; BF, bare fallow; A, continuous arable rotation; LA, ley-arable rotation; G, grass; P_T^{Core} , soil total porosity; P_T^{CT} , total X-ray micro-CT resolvable porosity; P_I^{CT} , isolated porosity; P_C^{CT} , surface connected porosity; S_p , surface density; Euler, Euler values; V_S , solid volume; A_S , surface area; L_D , equivalent sphere diameter; l_1 , shortest length; l_2 , intermediate length; l_3 , longest length; L , equivalent cubic length; l_1/l_3 , ratio's l_1 to l_3 ; l_2/l_3 , ratio's l_2 to l_3 ; L_B , average branch length; S , sphericity; S_E , sphericity of ellipsoidal objects.

* Corresponding author.

E-mail address: jlj@agro.au.dk (J.L. Jensen).

<https://doi.org/10.1016/j.geoderma.2025.117357>

Received 31 January 2025; Received in revised form 12 May 2025; Accepted 18 May 2025

Available online 21 May 2025

0016-7061/© 2025 The Authors. Published by Elsevier B.V. This is an open access article under the CC BY license (<http://creativecommons.org/licenses/by/4.0/>).

size, the function of aggregates in SOC protection and stabilization varies with their structural features (Oades and Waters, 1991; Six and Paustian, 2014). Therefore, the issue of aggregate size should be considered, since the shape or arrangement of various-sized aggregate clusters may affect soil aeration (such as soil porosity) and SOC sequestration, which in turn influence SOC storage (Regelink et al., 2015; Schlüter et al., 2022).

The formation and structure of soil aggregates are susceptible to soil management practices due to changes in carbon input and mechanical disturbance (such as tillage) (Dal Ferro et al., 2014; Zhang et al., 2021). Generally, soils with higher SOC have improved soil structural stability (Jensen et al., 2019a; Qi et al., 2022). Moreover, large aggregates are expected to be more sensitive to soil management than smaller aggregates as they are less stable and more influenced by dynamics in carbon input/root growth (Zhang et al., 2023; Dal Ferro et al., 2023). A study on sandy loam soil from Askov (DK) showed that the inclusion of cover crop to some extent ($P = 0.054$) decreased the stability of 8–16 mm diameter aggregates, while no effect was seen for 1–2 mm aggregates ($P = 0.694$) (Qi et al., 2022). Obour et al. (2018) found that 8–16 mm aggregates had lower tensile strength, but higher elasticity compared to 2–4 mm aggregates, and there was a negative linear decrease in aggregate tensile strength with increasing SOC across three aggregate size classes (8–16, 4–8, and 1–2 mm). These studies focus on the strength and stability parameters of aggregates and their correlations to SOC based on tension test and clay dispersibility but disregard aggregate shape and pore characteristics. Munkholm et al. (2016) and Winstone et al. (2019) quantified the 3D aggregate characteristics in terms of strength, shape, porosity, and radiodensity, whereas they did not associate the aggregate structural characteristics with SOC. To improve the understanding of interaction mechanisms between SOC and aggregates, more attention needs to be paid to further assessing the relationships between SOC and aggregate structural characteristics from the perspective of pore and shape characteristics.

It is well known that inter-aggregate and intra-aggregate porosity plays an important role in regulating the fate of SOC, in turn, SOC also acts as an essential contributor to shaping soil aggregation and aggregate pore structure (Kravchenko and Guber, 2017; Yudina and Kuzya-kov, 2023). This paper will evaluate the pore and shape characteristics of soil aggregates under different long-term soil management and their relationships with SOC based on soil from the Highfield Ley-Arable Long-Term Experiment (Highfield-LTE). Thus, the paper takes offset in an “aggregate approach” to study soil structure but with linkages to previously published soil properties derived from intact soil cores “pore approach” (Jensen et al., 2019b and 2020a). The objectives of this study were: 1. To quantify the pore and shape properties of differently sized aggregates as affected by contrasting long-term soil management; 2. To analyze the relationships between pore and shape properties of differently sized aggregates and SOC. Our hypotheses were: 1. Soil management has strong effects on aggregate pore and shape properties, which is related to changes in SOC. 2. Pore and shape properties of large aggregates are more sensitive to soil management than those of small aggregates.

2. Materials and methods

2.1. Experimental site and treatments

The Highfield-LTE (51°80'N, 00°36'W) was established in 1949 at Rothamsted Research (Harpenden, UK). The soil is a silt loam and is classified as a Chromic Luvisol according to the World Reference Base (WRB) soil classification system (Watts and Dexter, 1997). Four treatments were selected from Highfield-LTE: (i) bare fallow (BF) cultivated 2–4 times per year since 1959; (ii) continuous arable rotation (A) with winter cereals and ploughed once a year since 1949; (iii) ley-arable rotation (LA) with a 3-yr grass-clover ley followed by 3-yr arable management (ploughed annually when arable) since 1949; (iv) grass (G)

with predominantly grass and absence of tillage since 1949. Two of the plots from the LA treatment were drilled with winter cereals following three years of grass/clover, while the other two were drilled with grass/clover following three years of winter cereals. The A, LA, and G treatments were part of a randomized block design with four field replicates, whereas the four BF plots were located at one end of the experimental site. For a more detailed description of the experimental site and soil management see Jensen et al. (2019a; 2019b).

Soil was sampled in March 2015 at soil water content close to field capacity. For each replicate plot, three soil blocks (2750 cm³) were carefully retrieved from the 6–15 cm soil layer using a spade. The 0–6 cm depth was excluded to get rid of the dense grass root mat in the G treatment as well as the upper soil layer in the other treatments being largely heterogeneous as they encompassed contrasting management systems varying in tillage intensity and cropping. Thus, the sampling depth was chosen to get a more comparable basis for the tests. The soil samples were kept in sealed plastic boxes to prevent soil disturbance during transport and stored at 2 °C until required for analysis. Part of the field-moist soil samples were moved to steel trays, carefully fragmented by hand in several sittings along natural planes of weakness, and then allowed to air-dry at room temperature (~20 °C). The 2–4, 4–8, and 8–16 mm aggregates were obtained by sieving air-dried bulk soil as detailed in Obour et al. (2018). Each treatment had 24 air-dry aggregates randomly selected from each size class (2–4, 4–8, and 8–16 mm) for X-ray micro-CT scanning. The aggregates were gently transferred one by one to the holes of a cylinder containing 18 individual aggregates. The cylinder was separated into three layers with six holes in each. According to the aggregate size, 18 aggregates of three sizes from the same treatment were placed individually in the corresponding layers in each cylinder. Thus, the aggregates from each treatment (3 × 24) were scanned during four rounds. Previously published data by Jensen et al. (2019a; 2019b) and Jensen et al. (2020a) on SOC, soil texture, soil bulk density, and soil total porosity (P_{T}^{Core}) were used (Table 1).

2.2. CT scanning and image analysis

The cylinders with aggregates were scanned using a Nikon XTH 225 ST CT scanner (Museum of Ontario Archeology). The samples were scanned at 150 kV, 79 μA, 0.5 mm Cu filtering and with a 3500-millisecond integration time, generating an axial sequence of X-ray attenuation imagery with 40 μm pixel edge length. Image reconstruction was done using CT Pro 3D. The final reconstructed image had also a voxel edge length of 40 μm.

Image processing, visualization, and quantification were performed using an open-source software program Fiji/ImageJ (Schneider et al., 2012). For each cylinder scan, three regions of interest (ROI) were created containing one compartment, i.e. three layers in each cylinder.

Table 1

Basic soil characteristics under different treatments.

	BF	A	LA	G
SOC (g 100 g ⁻¹ minerals) ^a	0.90	1.73 ^{b*}	2.16 ^{b*}	3.29 ^{a*}
Clay < 2 μm (g 100 g ⁻¹ minerals) ^b	27	26	26	26
Fine silt 2–20 μm (g 100 g ⁻¹ minerals) ^b	25	26	26	27
Coarse silt 20–63 μm (g 100 g ⁻¹ minerals) ^b	33	32	32	32
Sand 63–2000 μm (g 100 g ⁻¹ minerals) ^b	15	16	16	15
Soil bulk density (g cm ⁻³) ^c	1.45	1.39 ^a	1.21 ^{b*}	1.13 ^{b*}
P_{T}^{Core} (m ³ m ⁻³) ^c	0.460	0.475 ^b	0.479 ^b	0.561 ^{a*}

The superscript lower-case letters denote statistical significance ($P < 0.05$) among A, LA and G treatments. A superscript asterisk (*) indicates if BF is significantly different from A, LA and G based on a pairwise *t*-test ($P < 0.05$). Abbreviations: BF: bare fallow, A: continuous arable rotation, LA: ley-arable rotation, G: grass, P_{T}^{Core} : soil total porosity.

^a Data from Jensen et al. (2019a).

^b Data from Jensen et al. (2019b).

^c Data from Jensen et al. (2020a).

That is each ROI contained six aggregates. The image analysis consisted of (i) normalization of the contrast/brightness to 0.35 % to eliminate brightness differences between image sequences using the ‘normalize’ command; (ii) application of a 3-pixel radius median filter in the ‘Filters’ command to reduce the noise, remove ring artifacts and improve contrast between the pore space and solids in images; (iii) image segmentation with a standardized/default and automated thresholding procedure; (iv) using a Particle Analyzer plugin provided by BoneJ to get general aggregate structure characteristics. The following settings were chosen: Thickness, surface area, enclosed volume, Euler characteristics, ellipsoids and skeletons. To obtain information on the entire volume of the aggregates (enclosed pore space as well as solid), we first applied the Binary operation ‘Fill Holes’ on 3D segmented images and then again used the Particle Analyzer operation with the above-mentioned settings. Volume visualization of the 3D aggregates was carried out using the ImageJ 3D viewer plug-in. The procedure was described in detail by

Munkholm et al. (2016). The segmented images and ‘Fill Holes’ images with 2D and 3D versions of aggregates were shown in Fig. 1. Examples of an isolated and a surface-connected pore at a 2D scale are marked as shown in Fig. 1a.

2.3. Aggregate pore parameters

Pore connectivity of each aggregate was derived from the ‘Fill Holes’ images and expressed by the Euler number (Dal Ferro et al., 2013; Bucka et al., 2019). The more negative the Euler number, the greater the pore connectivity. Based on the results from the segmented and ‘Fill Holes’ images, the total X-ray micro-CT (at 40 μm voxel size) resolvable porosity (P_T^{CT}) within aggregate, i.e. isolated plus surface connected, was estimated as suggested by Munkholm et al. (2016):

$$P_T^{CT} = (V_F - V_S)/V_F \quad (3)$$

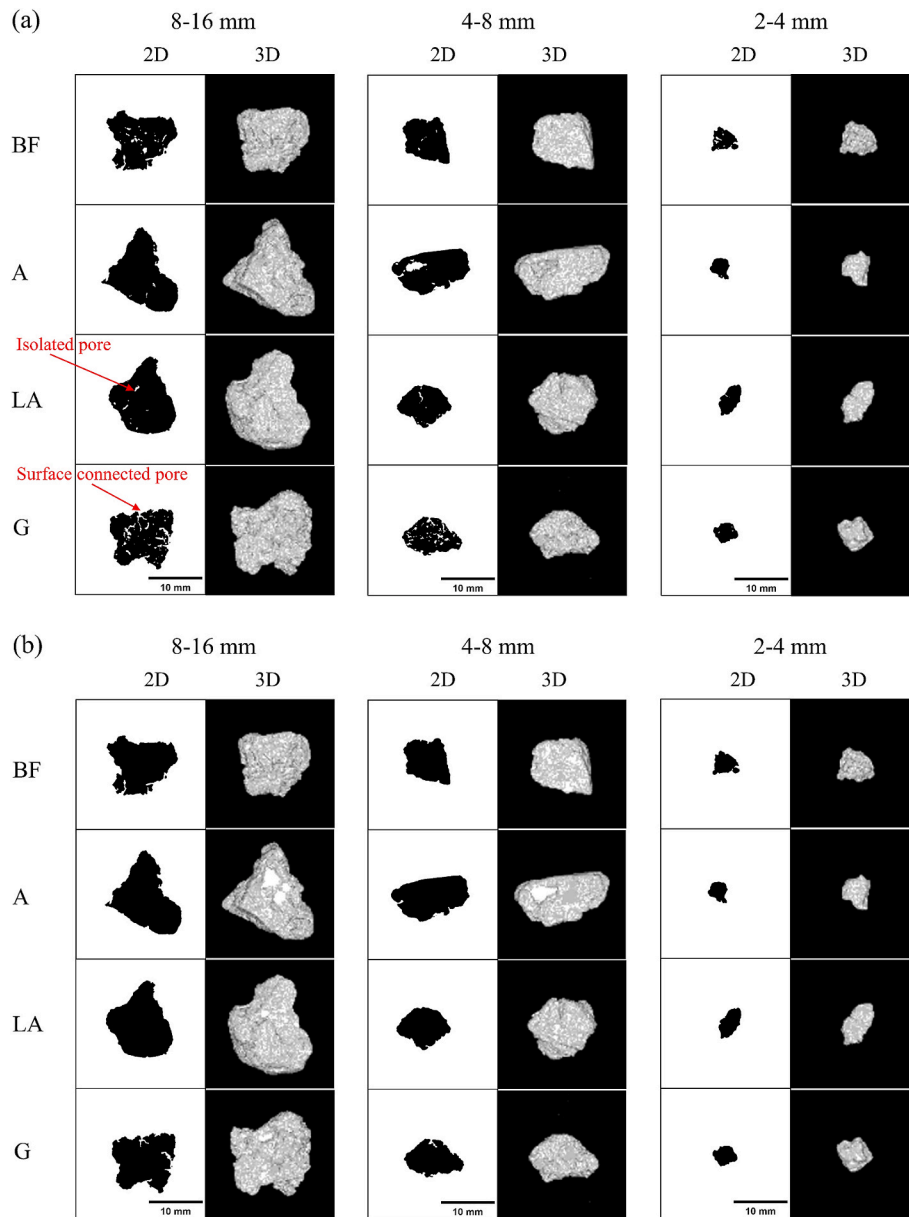


Fig. 1. 2D and 3D visualizations of soil aggregate from X-ray micro-CT scanning at 40 μm resolution. The aggregates were from treatments: bare fallow (BF), continuous arable rotation (A), ley-arable rotation (LA) and grass (G). Black and white areas in 2D visualizations of soil aggregate represent soil particle and pore space, respectively. (a): X-ray micro-CT scanning segmented image. (b): binary X-ray micro-CT scanning of ‘Fill Holes’ image. Examples of an isolated and a surface connected pore at 2D scale are marked.

where V_F is the enclosed voxels (solids and pores) from the 'Fill Holes' images and V_S is the number of solid voxels in the originally segmented images.

The isolated porosity (P_I^{CT}) of aggregate was derived from the segmented images and calculated as:

$$P_I^{CT} = 1 - V_S/V_{SE} \quad (4)$$

where V_{SE} is the number of enclosed voxels (solids and pores) in the originally segmented images.

The surface-connected porosity (P_C^{CT}) of aggregate was calculated as:

$$P_C^{CT} = P_T^{CT} - P_I^{CT} \quad (5)$$

The surface density (S_D) represents the proportion of transition from pores to solids (Bacq-Labreuil et al., 2018). It was determined as:

$$S_D = A_S/V_S \quad (6)$$

where A_S is the surface area (mm^2) and V_S is the number of solid volumes (mm^3) in the originally segmented images.

2.4. Aggregate shape parameters

In most cases, aspect ratios of aggregates are closer to cubes than to spheres. The equivalent cubic length (L) is regarded as an appropriate shape parameter according to Perfect et al. (1997).

$$L = \sqrt[3]{l_1(l_2/\sqrt{2})(l_3/\sqrt{3})} \quad (7)$$

where l_1 , l_2 , and l_3 are the shortest, intermediate, and longest lengths of each single aggregate determined from the 'Fill Holes' images.

The sphericity (S) of the aggregates was determined according to Wadell (1935):

$$S = \left[\frac{\frac{1}{\pi^3}(6V_F)^{\frac{2}{3}}}{A_F} \right] \quad (8)$$

where A_F is the aggregated surface area derived from the 'Fill Holes' images.

The sphericity of ellipsoidal objects (S_E) is complementary to S , which was calculated as suggested by Sneed and Folk (1958):

$$S_E = \sqrt[3]{l_1^2/l_2l_3} \quad (9)$$

Solid volume (V_S) and surface area (A_S) were derived from the originally segmented images. Other aggregate shape parameters, such as equivalent sphere diameter (L_D) and average branch length (L_B), were determined from the 'Fill Holes' images (Katuwal et al., 2015).

2.5. Statistical analysis

Treatment differences and Pearson's correlation analysis were carried out in the R software package (R Core Team, 2022). Treatment differences for the comparison among A, LA, and G treatments were analyzed with a linear mixed model including block as a random effect. Statistical significance was determined at the 95 % confidence level. When the treatment effect was significant ($P < 0.05$), further analyses were made to isolate differences between treatments (pairwise comparisons) using the general linear hypotheses (glht) function implemented in the R 'multcomp' package. The degree of freedom was calculated by the Kenward-Roger method (Kenward and Roger, 2009). Since the BF treatment is not a part of the original ley-arable experiment, we applied a pairwise t-test (a less robust test) to compare the treatment differences between BF and other treatments. Pearson's correlation was performed to obtain the relationships between soil aggregate pore and

shape characteristics using the R 'corrplot' package. Linear regression relationships between SOC and aggregate structural characteristics were organized by Origin 9.1 (Origin Lab Corporation, Northampton, USA).

3. Results

3.1. Basic soil characteristics

The SOC concentration under G was significantly higher than LA, A, and BF (Table 1). Additionally, G resulted in soil total porosity (P_T^{Core}) values that were 17–22 % higher and soil bulk density values that were 4–27 % lower than those observed under the other treatments. No significant treatment effect was observed for clay, silt, and sand content.

3.2. Aggregate pore characteristics

For the larger 8–16 mm aggregates, the total X-ray CT resolvable porosity (P_T^{CT}), isolated porosity (P_I^{CT}), surface connected porosity (P_C^{CT}), and surface density (S_D) differed significantly and decreased in the order $G > LA > BF > A$ (Table 2). Similarly, higher P_T^{CT} , P_C^{CT} , and S_D for 4–8 mm aggregates were observed under G relative to the other treatments and did not differ significantly among LA, A, and BF treatments. For smaller 2–4 mm aggregates, there were no significant treatment effects, although P_T^{CT} , P_C^{CT} , and S_D tended to decrease in the order $G > LA > A$. The G resulted in a significantly higher P_I^{CT} (82 %) than BF for 2–4 mm aggregates. Additionally, the Euler values were lowest across three aggregate size classes under G relative to the other treatments and tended to increase in the order $G < LA < A$ (especially for 8–16 mm and 4–8 mm aggregates).

3.3. Aggregate shape characteristics

For 8–16 mm and 4–8 mm aggregates, solid volume (V_S), equivalent sphere diameter (L_D), intermediate (l_2) and longest (l_3) length, equivalent cubic length (L), average branch length (L_B), and sphericity (S) increased in the order $G < LA < A$, whereas the ratios of shortest (l_1) to l_3 (l_1/l_3), and l_2 to l_3 (l_2/l_3) and sphericity of ellipsoidal objects (S_E) presented opposite tendencies (Table 3). The values of L_D and S within 8–16 mm and 4–8 mm aggregates for BF were significantly 20–35 % and 11–16 % higher than for G, respectively. Significant differences between

Table 2

Aggregate pore properties as influenced by different long-term treatments. The pore characteristics are derived from X-ray micro-CT scanning of aggregates.

	P_T^{CT} (%)	P_I^{CT} (%)	P_C^{CT} (%)	S_D ($\text{mm}^2 \text{mm}^{-3}$)	Euler values
8–16 mm					
BF	2.53	0.41	2.12	1.18	−16.33
A	1.18 ^c	0.29 ^b	0.89 ^c	1.08 ^c	−14.79 ^a
LA	2.32 ^b	0.42 ^{ab}	1.90 ^b	1.32 ^b	−22.17 ^a
G	3.49 ^a	0.59 ^a	2.90 ^a	1.68 ^{a*}	−72.71 ^{b*}
4–8 mm					
BF	1.24	0.50	0.74	1.69	−2.46
A	1.49 ^b	0.57	0.92 ^b	1.59 ^b	−3.96 ^a
LA	1.74 ^b	0.51	1.23 ^b	1.80 ^b	−5.71 ^a
G	3.03 ^{a*}	0.71	2.32 ^{a*}	2.13 ^{a*}	−15.46 ^{b*}
2–4 mm					
BF	0.93	0.59	0.33	3.20	0.50
A	0.94	0.76	0.19	3.15	0.92 ^a
LA	1.32	0.77	0.55	3.14	−0.22 ^b
G	1.68	1.07 [*]	0.60	3.25	−0.38 ^b

The superscript lower-case letters denote statistical significance ($P < 0.05$) among A, LA and G treatments. A superscript asterisk (*) indicates if BF is significantly different from A, LA and G based on a pairwise t-test ($P < 0.05$). Abbreviations: BF: bare fallow, A: continuous arable rotation, LA: ley-arable rotation, G: grass, P_T^{CT} : total X-ray micro-CT resolvable porosity, P_I^{CT} : isolated porosity, P_C^{CT} : surface connected porosity, S_D : surface density, Euler: Euler values.

Table 3

Aggregate shape properties as influenced by different long-term treatments. The shape characteristics are derived from X-ray micro-CT scanning of aggregates.

	V_s (mm ³)	A_s (mm ²)	L_D (mm)	l_1 (mm)	l_2 (mm)	l_3 (mm)	L (mm)	l_1/l_3	l_2/l_3	L_B (mm)	S	S_E
8–16 mm												
BF	540.81	611.45	8.07	7.42	10.93	15.48	7.95	0.49	0.72	1.14	0.63	0.69
A	536.66	569.35	8.01 ^a	7.22	10.63	23.75	8.45 ^a	0.44	0.64 ^b	1.14 ^a	0.63 ^a	0.66
LA	493.41	624.01	6.98 ^{ab}	7.31	10.48	15.56	7.80 ^{ab}	0.49	0.69 ^b	1.08 ^{ab}	0.59 ^a	0.70
G	446.98	737.82	5.99 ^{b*}	6.95	9.83 [*]	13.76	7.24 ^b	0.52	0.73 ^a	0.99 ^{b*}	0.54 ^{b*}	0.71
4–8 mm												
BF	105.68	172.32	4.90	4.12	6.42	9.07	4.57	0.47	0.72	0.87	0.66	0.67
A	140.96 ^{a*}	222.00 [*]	5.17 ^a	4.38	6.62	11.69 ^{a*}	4.12 ^{a*}	0.39 ^b	0.59 ^{b*}	0.92	0.64	0.64
LA	122.02 ^{ab}	212.66	4.65 ^{ab}	4.35	6.46	10.12 ^b	4.85 ^{ab}	0.44 ^{ab}	0.65 ^{ab}	0.89	0.61	0.67
G	111.28 ^b	227.41 [*]	4.08 ^{b*}	4.30	6.17	9.24 ^b	4.61 ^b	0.48 ^a	0.69 ^a	0.86	0.59 [*]	0.69
2–4 mm												
BF	10.95	33.45	2.47	1.87	2.87	4.49	2.12	0.44	0.67	0.68	0.73	0.66
A	10.94	31.42 ^b	2.59	1.84	2.89	4.42 ^b	2.11	0.43 ^{ab}	0.67 ^{ab}	0.67	0.74 ^a	0.65
LA	15.55	44.34 ^a	2.49	2.06	3.08	5.18 ^a	2.35	0.41 ^b	0.61 ^b	0.65	0.68 ^b	0.64
G	11.70	35.11 ^{ab}	2.49	1.97	2.91	4.10 ^b	2.11	0.49 ^a	0.71 ^a	0.63	0.73 ^a	0.70

The superscript lower-case letters denote statistical significance ($P < 0.05$) among A, LA and G treatments. A superscript asterisk (*) indicates if BF is significantly different from A, LA and G based on a pairwise t -test ($P < 0.05$). Abbreviations: BF: bare fallow, A: continuous arable rotation, LA: ley-arable rotation, G: grass, V_s : solid volume, A_s : surface area, L_D : equivalent sphere diameter, l_1 : shortest length, l_2 : intermediate length, l_3 : longest length, L : equivalent cubic length, l_1/l_3 : ratio's l_1 to l_3 , l_2/l_3 : ratio's l_2 to l_3 , L_B : average branch length, S : sphericity, S_E : sphericity of ellipsoidal objects.

BF and A were also observed for V_s , surface area (A_s), l_3 , L , and l_2/l_3 values for 4–8 mm aggregates. The general pattern differed for 2–4 mm aggregates as LA had the largest values of V_s , A_s , l_1 , l_2 , l_3 , and L , as well

as the smallest values of l_1/l_3 , l_2/l_3 , S , and S_E . Additionally, shape characteristics of 2–4 mm aggregate did not differ significantly between BF and other treatments.

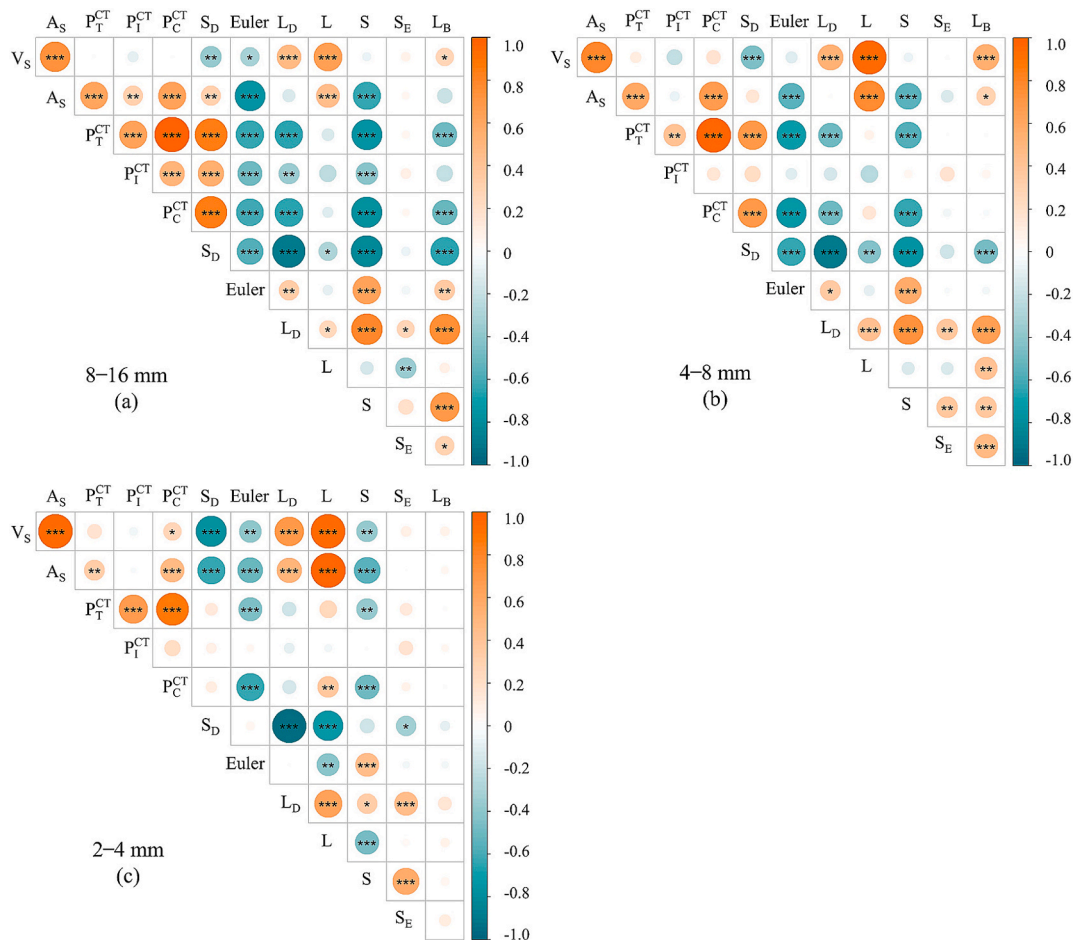


Fig. 2. Relationships between aggregate pore and shape properties for 8–16 mm aggregates (a), 4–8 mm aggregates (b) and 2–4 mm aggregates (c). The color and size of the circles indicate the sign (orange and blue colors indicate positive and negative correlations, respectively) and strength (the intensity of the color) of the correlation. *, **, and *** mean significant at the 0.05, 0.01 and 0.001 level, respectively. Abbreviations: V_s : solid volume, A_s : surface area, P_T^{CT} : total X-ray micro-CT resolvable porosity, P_I^{CT} : isolated porosity, P_C^{CT} : surface connected porosity, S_D : surface density, Euler: Euler values, L_D : equivalent sphere diameter, L : equivalent cubic length, S : sphericity, S_E : sphericity of ellipsoidal objects, L_B : average branch length.

3.4. Relationships between aggregate pore and shape characteristics

The relationships between aggregate pore and shape characteristics were affected by aggregate size (Fig. 2). For all size classes of aggregates, A_S was positively correlated with P_T^{CT} , P_C^{CT} , and L ($r \geq 0.3$, $P < 0.01$), but negatively correlated with Euler values and S ($r \leq -0.5$, $P < 0.01$). Additionally, L_D was positively correlated with L , S , and S_E ($r \geq 0.2$, $P < 0.05$) but negatively correlated with S_D ($r \leq -0.9$, $P < 0.01$) for all sizes of aggregates. Meanwhile, Euler values were positively correlated with S ($r \geq 0.5$, $P < 0.01$) and the correlation coefficient decreased with increasing aggregate size. Moreover, S_D was negatively correlated with L_D and L ($r \leq -0.3$, $P < 0.01$), and the correlation coefficient decreased with increasing aggregate size. Significant correlations of L_B with S_E and S were also found for 8–16 mm and 4–8 mm aggregates ($r \geq 0.3$, $P <$

0.05). The correlations of P_T^{CT} and P_C^{CT} with Euler values, L_D , S , and S_D for 2–4 mm aggregates were weaker than for 8–16 mm and 4–8 mm aggregates.

3.5. Linking aggregate structure characteristics to SOC

We observed that P_T^{CT} had a significant and positive relationship with SOC for 4–8 mm aggregates ($R^2 = 0.51$, $P = 0.002$) (Fig. 3). For 8–16 mm aggregates, Euler values and S were highly and negatively related with SOC ($R^2 \geq 0.25$, $P < 0.05$), which correspond to slopes of -18.2 and -0.031 per $\text{g } 100 \text{ g}^{-1}$ minerals increase in SOC concentration, respectively. Similar relationships were found for 4–8 mm aggregates, but the slopes of the linear relationships with SOC were lower than for 8–16 mm aggregates, corresponding to slopes of -5.1 ($R^2 = 0.61$, $P < 0.001$) and

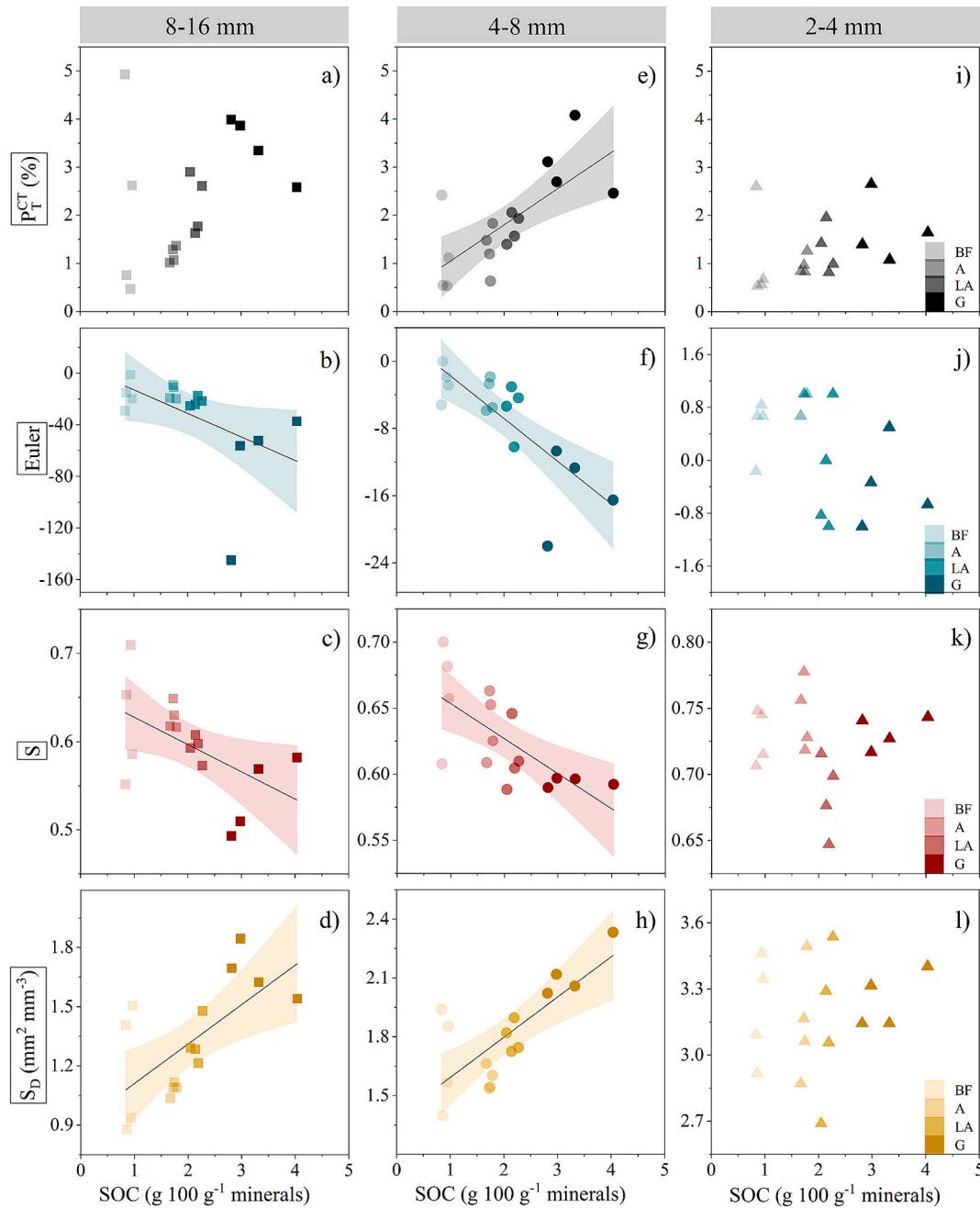


Fig. 3. The soil aggregate properties as a function of soil organic carbon (SOC) for 8–16 mm aggregates (a–d), 4–8 mm aggregates (e–h) and 2–4 mm aggregates (i–l). Color band represents the 95 % confidence interval. Abbreviations: BF: bare fallow, A: continuous arable rotation, LA: ley-arable rotation, G: grass, P_T^{CT} : total X-ray micro-CT resolvable porosity, Euler: Euler values, S : sphericity, S_D : surface density.

-0.027 ($R^2 = 0.47$, $P = 0.003$) per $\text{g } 100 \text{ g}^{-1}$ minerals increase in SOC concentration, respectively. However, S_D was significant and positively related to SOC for 8–16 mm and 4–8 mm aggregates ($R^2 \geq 0.43$, $P < 0.01$). Surprisingly, no significant linear relationships were found between aggregate structure characteristics and SOC for 2–4 mm aggregates.

4. Discussion

4.1. Soil management effects

Our results showed significant effects of soil management, especially positive effects of permanent grass (G) vs. ley-arable (LA), arable (A), and bare fallow (BF) management, on soil total porosity (P_T^{Core}), aggregate pore and shape characteristics (P_T^{CT} , P_C^{CT} , S_D , Euler values, L_D , L , and S) (Tables 1, 2, and 3), supporting our first hypothesis. This suggested that soil management affected both inter- and intra-aggregate pore space (Munkholm et al., 2016), which may be ascribed to differences in both organic carbon inputs and tillage (Dal Ferro et al., 2014; Zhang et al., 2023). The greater aggregate porosity and pore connectivity observed under G compared to BF indicated that G promoted a well-connected pore network for aggregates, related to the greater plant-derived carbon inputs and the absence of tillage (Bacq-Labreuil, et al., 2018; Jensen et al., 2019a and 2020a). This result supported findings from Zhang et al. (2021) and Wang et al. (2022), who also found that G increased pore connectivity and fluid transport capabilities of soil aggregates analyzed with X-ray at $1.5 \mu\text{m}$ resolution at the same experimental site.

The effects of treatment on aggregate structural characteristics demonstrated that greater SOC concentration – due to high organic carbon inputs under the LA and especially G treatments – had aggregates with a more open and well-connected pore structure, rougher surfaces and a more spherical shape (especially so for larger aggregates) (Munkholm et al., 2016; Dal Ferro et al., 2023). Previous studies have also shown strong effects of the long-term management on the stability of 1–2 mm and 8–16 mm aggregates from the same experiment (Jensen et al., 2019a; 2020b). It has also been shown that organic inputs from above- and belowground plant residues promote aggregate bonding (e.g. labile soil carbon) and binding agents (e.g. fungal hyphae) (Elmholt et al., 2008; Kravchenko et al., 2021), and thereby affect aggregate pore, shape, and stability characteristics (Elmholt et al., 2008; Kravchenko et al., 2019; Yudina and Kuzyakov, 2023). In turn, more porous aggregates with rough surfaces afford more adsorption sites for SOC and improve living conditions for microorganisms and their associated products (such as fungal hyphae and exoenzymes) (Regelink et al., 2015; Schlüter et al., 2020; Wang et al., 2022). Studies by Hirsch et al. (2009), Hirsch et al. (2017) and Neal et al. (2021) from the Highfield experiment confirmed that the treatments with greater carbon inputs – thereby greater SOC concentration and favorable physical habitats for soil biota – fostered increased microbial activity.

Further, the well-developed structure in the soils with greater organic matter input (i.e. LA and G) are of key importance for carbon stabilization (Tao et al., 2023), who concluded that a well-structured soil benefited microbial carbon use efficiency and thus soil carbon storage via microbial necromass. Yudina and Kuzyakov (2023) also highlighted that soils with a well-developed hierarchical soil structure provided both sites (e.g. in macro- and meso-aggregates) with favorable conditions for microbial-derived decomposition products as well as sites (e.g. in microaggregates) for carbon stabilization via organo-mineral interactions.

Notably, these observed treatment effects on aggregate pore and shape characteristics mainly existed in 8–16 mm and 4–8 mm aggregates but not in 2–4 mm aggregates (Tables 2 and 3). This agrees with Obour et al. (2018) and Jensen et al. (2020b), who found the more pronounced management effects on soil structural stability and aggregate strength with increasing aggregate size from the same experiment. Qi et al.

(2022) also reported that the inclusion of cover crop did not affect the stability of 1–2 mm aggregates but increased the stability of 8–16 mm aggregates. They considered that this difference was attributed to a larger amount of binding agents from cover crops such as roots, thus resulting in a more active function in stabilizing larger aggregates.

4.2. Aggregate size effects

Specifically, we observed that P_T^{CT} increased with increasing aggregate size, whereas Euler values, S_D , and S decreased with increasing aggregate size (Tables 2 and 3). In addition, the relationships among P_T^{CT} , Euler values, S_D , and S were stronger for 8–16 mm and 4–8 mm aggregates than 2–4 mm aggregates (Fig. 2). These results indicate that structural characteristics of large aggregates were more complex, which was likely linked to the hierarchical aggregation process as affected by carbon inputs and the degree of physical disturbance (Six and Paustian, 2014; Munkholm et al., 2016).

The difference in the response of aggregate pore and shape characteristics to soil management and SOC concentration between large size and small size might be explained as follows: Firstly, soil with a high SOC concentration tends to hold more biotic binding and bonding agents (e.g. fungal hyphae and roots), promoting the formation of large aggregates from soil particles and small aggregates, thus resulting in higher aggregate porosity and greater pore connectivity (Munkholm et al., 2002; Dal Ferro et al., 2023). Secondly, large aggregates have lower tensile strength and specific rupture energy, hence they are much more easily influenced by soil management such as tillage (Munkholm and Kay, 2002; Obour et al., 2018). In addition, pore connectivity (i.e. Euler values) and sphericity (S) were more strongly influenced by SOC (i.e. greater slope) in larger aggregates (Fig. 3). These results suggest that the pore and shape characteristics of large aggregates were significantly linked to soil carbon processes, which is consistent with Kravchenko and Guber (2017) in terms of the soil pore characteristics.

5. Conclusions

The Highfield-LTE, encompassing bare fallow, continuous arable rotation, ley-arable rotation, and grass treatments, enabled the quantification of pore and shape characteristics of soil aggregates at various hierarchical levels subjected to different long-term soil management practices. The results showed that pore connectivity of soil aggregates increased for the grass treatment as compared to bare fallow or arable across different aggregate size classes (2–4, 4–8, and 8–16 mm). The treatments had a significant effect on the pore and shape characteristics of aggregates in the 8–16 mm and 4–8 mm size classes, but not in the 2–4 mm class. Based on our results, we assumed that the primary drivers in play were organic carbon inputs and mechanical disturbance (tillage). Moreover, the relationships between SOC and aggregate structural characteristics were strong for 8–16 mm and 4–8 mm aggregates, but weak for 2–4 mm aggregates. The results highlight the need for more knowledge on the complex interactions between soil structure and carbon dynamics at different hierarchical scales.

CRediT authorship contribution statement

Weijun Zhang: Writing – original draft, Visualization, Formal analysis, Data curation, Conceptualization. **Lars J. Munkholm:** Writing – review & editing, Supervision, Project administration, Methodology, Funding acquisition, Conceptualization. **Richard J. Heck:** Writing – review & editing, Software, Resources, Methodology. **Christopher W. Watts:** Writing – review & editing, Resources, Conceptualization. **Johannes L. Jensen:** Writing – review & editing, Supervision, Investigation, Conceptualization.

Declaration of competing interest

The authors declare that they have no known competing financial interests or personal relationships that could have appeared to influence the work reported in this paper.

Acknowledgements

The authors gratefully acknowledge the technical assistance of Stig T. Rasmussen, Dept. Agroecology (Aarhus University), and the technical staff at Rothamsted Research. Thanks to Prof. Jingkuan Wang (College of Land and Environment, Shenyang Agricultural University) for his contribution to obtaining the scholarship from China Scholarship Council for Weijun Zhang and facilitate this collaboration. The study was supported by the Green Development and Demonstration Programme (GUDP) of the Ministry of Environment and Food of Denmark through the “Cover crops for optimization of cereal based cropping systems” (Grant No. 3405-11-0225) and “Optimized soil tillage in cereal based cropping systems” (Grant No. 34009-12-0502) projects, and by the EU 7th Research Framework Programme, Distributed Infrastructure for Experimentation in Ecosystem Research (ExpeER) through the project “Identification of soil organic carbon thresholds for sustained soil functions in agroecosystems” (Grant No. 262060). The Highfield LTE is part of the Rothamsted Long-Term Experiments National Bioscience Research Infrastructure, supported by UK Research and Innovation – Biotechnology and Biological Sciences Research Council (UKRI-BBSRC) (grant code BBS/E/RH/23NB0007) and the Lawes Agricultural Trust.

Data availability

Data will be made available on request.

References

- Bacq-Labreuil, A., Crawford, J., Mooney, S.J., Neal, A.L., Akkari, E., McAuliffe, C., Zhang, X., Redmile-Gordon, M., Ritz, K., 2018. Effects of cropping systems upon the three-dimensional architecture of soil systems are modulated by texture. *Geoderma* 332, 73–83. <https://doi.org/10.1016/j.geoderma.2018.07.002>.
- Bucka, F.B., Kölbl, A., Uteau, D., Peth, S., Kögel-Knabner, I., 2019. Organic matter input determines structure development and aggregate formation in artificial soils. *Geoderma* 354, 113881. <https://doi.org/10.1016/j.geoderma.2019.113881>.
- Dal Ferro, N., Charrier, P., Morari, F., 2013. Dual-scale micro-CT assessment of soil structure in a long-term fertilization experiment. *Geoderma* 204–205, 84–93. <https://doi.org/10.1016/j.geoderma.2013.04.012>.
- Dal Ferro, N., Sartori, L., Simonetti, G., Berti, A., Morari, F., 2014. Soil macro- and microstructure as affected by different tillage systems and their effects on maize root growth. *Soil Tillage Res.* 140, 55–65. <https://doi.org/10.1016/j.still.2014.02.003>.
- Dal Ferro, N., Stevenson, B., Morari, F., Müller, K., 2023. Long-term tillage and irrigation effects on aggregation and soil organic carbon stabilization mechanisms. *Geoderma* 432, 116398. <https://doi.org/10.1016/j.geoderma.2023.116398>.
- Elmholt, S., Schjønning, P., Munkholm, L.J., Deboz, K., 2008. Soil management effects on aggregate stability and biological binding. *Geoderma* 144, 455–467. <https://doi.org/10.1016/j.geoderma.2007.12.016>.
- Hirsch, P.R., Gilliam, L.M., Sohi, S.P., Williams, J.K., Clark, I.M., Murray, P.J., 2009. Starving the soil of plant inputs for 50 years reduces abundance but not diversity of soil bacterial communities. *Soil Biol. Biochem.* 41, 2021–2024. <https://doi.org/10.1016/j.soilbio.2009.07.011>.
- Hirsch, P.R., Jhurrea, D., Williams, J.K., Murray, P.J., Scott, T., Misselbrook, T.H., Goulding, K.W.T., Clark, I.M., 2017. Soil resilience and recovery: rapid community responses to management changes. *Plant and Soil* 412, 283–297. <https://doi.org/10.1007/s11004-016-3068-x>.
- Jensen, J.L., Schjønning, P., Watts, C.W., Christensen, B.T., Peltre, C., Munkholm, L.J., 2019a. Relating soil C and organic matter fractions to soil structural stability. *Geoderma* 337, 834–843. <https://doi.org/10.1016/j.geoderma.2018.10.034>.
- Jensen, J.L., Schjønning, P., Watts, C.W., Christensen, B.T., Munkholm, L.J., 2019b. Soil water retention: Uni-modal models of pore-size distribution neglect impacts of soil management. *Soil Sci. Soc. Am. J.* 83 (1), 18–26. <https://doi.org/10.2136/sssaj2018.06.0238>.
- Jensen, J.L., Schjønning, P., Watts, C.W., Christensen, B.T., Munkholm, L.J., 2020a. Short-term changes in soil pore size distribution: Impact of land use. *Soil Tillage Res.* 199, 104597. <https://doi.org/10.1016/j.still.2020.104597>.
- Jensen, J.L., Schjønning, P., Watts, C.W., Christensen, B.T., Obour, P.B., Munkholm, L.J., 2020b. Soil degradation and recovery—Changes in organic matter fractions and structural stability. *Geoderma* 364, 114181. <https://doi.org/10.1016/j.geoderma.2020.114181>.
- Katuwal, S., Norgaard, T., Moldrup, P., Lalandé, M., Wildenschild, D., de Jonge, L.W., 2015. Linking air and water transport in intact soils to macropore characteristics inferred from X-ray computed tomography. *Geoderma* 237, 9–20. <https://doi.org/10.1016/j.geoderma.2014.08.006>.
- Kenward, M.G., Roger, J.H., 2009. An improved approximation to the precision of fixed effects from restricted maximum likelihood. *Comput. Stat. Data Anal.* 53 (7), 2583–2595. <https://doi.org/10.1016/j.csda.2008.12.013>.
- Kravchenko, A.N., Guber, A.K., 2017. Soil pores and their contributions to soil carbon processes. *Geoderma* 287, 31–39. <https://doi.org/10.1016/j.geoderma.2016.06.027>.
- Kravchenko, A.N., Guber, A.K., Razavi, B.S., Koestel, J., Quigley, M.Y., Robertson, G.P., Kuzyakov, Y., 2019. Microbial spatial footprint as a driver of soil carbon stabilization. *Nat. Commun.* 10 (1), 1–10. <https://doi.org/10.1038/s41467-019-11057-4>.
- Kravchenko, A.N., Zheng, H., Kuzyakov, Y., Robertson, G.P., Guber, A.K., 2021. Belowground interplant carbon transfer promotes soil carbon gains in diverse plant communities. *Soil Biol. Biochem.* 159, 108297. <https://doi.org/10.1016/j.soilbio.2021.108297>.
- Munkholm, L.J., Heck, R.J., Deen, B., Zidar, T., 2016. Relationship between soil aggregate strength, shape and porosity for soils under different long-term management. *Geoderma* 268, 52–59. <https://doi.org/10.1016/j.geoderma.2016.01.005>.
- Munkholm, L.J., Kay, B.D., 2002. Effect of water regime on aggregate-tensile strength, rupture energy, and friability. *Soil Sci. Soc. Am. J.* 66, 702–709. <https://doi.org/10.2136/sssaj2002.7020>.
- Munkholm, L.J., Schjønning, P., Deboz, K., Jensen, H.E., Christensen, B.T., 2002. Aggregate strength and mechanical behaviour of a sandy loam soil under long-term fertilization treatments. *Eur. J. Soil Sci.* 53, 129–137. <https://doi.org/10.1046/j.1365-2389.2002.00424.x>.
- Neal, A.L., Hughes, D., Clark, I.M., Jansson, J.K., Hirsch, P.R., 2021. Microbiome aggregated traits and assembly are more sensitive to soil management than diversity. *mSystems*. 6 (3), 10–1128. <https://doi.org/10.1128/mSystems.01056-20>.
- Oades, J.M., Waters, A.G., 1991. Aggregate Hierarchy in Soils. *Soil Res.* 29, 815–828. <https://doi.org/10.1071/SR9910815>.
- Obour, P.B., Jensen, J.L., Lalandé, M., Watts, C.W., Munkholm, L.J., 2018. Soil organic matter widens the range of water contents for tillage. *Soil Tillage Res.* 182, 57–65. <https://doi.org/10.1016/j.still.2018.05.001>.
- Perfect, E., Zhai, Q., Blevins, R.L., 1997. Soil and tillage effects on the characteristic size and shape of aggregates. *Soil Sci. Soc. Am. J.* 61, 1459–1465. <https://doi.org/10.2136/sssaj1997.03615995006100050025x>.
- Qi, J., Jensen, J.L., Christensen, B.T., Munkholm, L.J., 2022. Soil structural stability following decades of straw incorporation and use of ryegrass cover crops. *Geoderma* 406, 115463. <https://doi.org/10.1016/j.geoderma.2021.115463>.
- R Core Team, 2022. R: A Language and Environment for Statistical Computing. R Foundation for Statistical Computing, Vienna, Austria. www.R-project.org.
- Regelink, I.C., Stoof, C.R., Rousseva, S., Weng, L., Lair, G.J., Kram, P., Nikolaidis, N.P., Kercheva, M., Banwart, S., Comans, R.N., 2015. Linkages between aggregate formation, porosity and soil chemical properties. *Geoderma* 247, 24–37. <https://doi.org/10.1016/j.geoderma.2015.01.022>.
- Schlüter, S., Leuther, F., Albrecht, L., Hoeschen, C., Kilian, R., Surey, R., Mikutta, R., Kaiser, K., Mueller, C.W., Vogel, H.J., 2022. Microscale carbon distribution around pores and particulate organic matter varies with soil moisture regime. *Nat. Commun.* 13 (1), 2098. <https://doi.org/10.1038/s41467-022-29605-w>.
- Schlüter, S., Sammartino, S., Koestel, J., 2020. Exploring the relationship between soil structure and soil functions via pore-scale imaging. *Geoderma* 370, 114370. <https://doi.org/10.1016/j.geoderma.2020.114370>.
- Schneider, C.A., Rasband, W.S., Eliceiri, K.W., 2012. NIH image to ImageJ: 25 years of image analysis. *Nat. Methods* 9, 671–675. <https://doi.org/10.1038/nmeth.2089>.
- Six, J., Paustian, K., 2014. Aggregate-associated soil organic matter as an ecosystem property and a measurement tool. *Soil Biol. Biochem.* 68, A4–A9. <https://doi.org/10.1016/j.soilbio.2013.06.014>.
- Sneed, E.D., Folk, R.L., 1958. Pebbles in the lower Colorado River, Texas a study in particle morphogenesis. *J. Geol.* 66, 114–150. <https://doi.org/10.1086/626490>.
- Tao, F., Huang, Y., Hungate, B.A., Manzoni, S., Frey, S.D., Schmidt, M.W., Reichstein, M., Carvalhais, N., Ciais, P., Jiang, L., Lehmann, J., Wang, Y.P., Houlton, Z.B., Ahrens, B., Mishra, U., Hugelius, G., Hocking, D.T., Lu, X., Shi, Z., Viatkin, K., Vargas, R., Yigini, Y., Omuto, C., Malik, A.A., Peralta, G., Cuevas, C.R.E., Di Paolo, L., Luotto, I., Liao, C., Liang, Y.S., Saynes, S.V., Huang, X., Luo, Y., 2023. Microbial carbon use efficiency promotes global soil carbon storage. *Nature* 618 (7967), 981–985. <https://doi.org/10.1038/s41586-023-06042-3>.
- Vogel, H.-J., Balseiro-Romero, M., Kravchenko, A., Otten, W., Pot, V., Schlüter, S., Weller, U., Baveye, P.C., 2022. A holistic perspective on soil architecture is needed as a key to soil functions. *Eur. J. Soil Sci.* 73 (1), e13152.
- Wadell, H., 1935. Volume, shape, and roundness of quartz particles. *J. Geol.* 43, 250–280. <https://doi.org/10.1086/624298>.
- Wang, F., Zhang, X., Neal, A.L., Crawford, J.W., Mooney, S.J., Bacq-Labreuil, A., 2022. Evolution of the transport properties of soil aggregates and their relationship with soil organic carbon following land use changes. *Soil Tillage Res.* 215, 105226. <https://doi.org/10.1016/j.still.2021.105226>.
- Watts, C.W., Dexter, A.R., 1997. The influence of organic matter in reducing the destabilization of soil by simulated tillage. *Soil Tillage Res.* 42 (4), 253–275. [https://doi.org/10.1016/S0167-1987\(97\)00009-3](https://doi.org/10.1016/S0167-1987(97)00009-3).

- Winstone, B.C., Heck, R.J., Munkholm, L.J., Deen, B., 2019. Characterization of soil aggregate structure by virtual erosion of X-ray CT imagery. *Soil Tillage Res.* 185, 70–76. <https://doi.org/10.1016/j.still.2018.09.001>.
- Yudina, A., Kuzyakov, Y., 2019. Saving the face of soil aggregates. *Glob. Chang. Biol.* 25 (11), 3574–3577. <https://doi.org/10.1111/gcb.14779>.
- Yudina, A., Kuzyakov, Y., 2023. Dual nature of soil structure: The unity of aggregates and pores. *Geoderma* 434, 116478. <https://doi.org/10.1016/j.geoderma.2023.116478>.
- Zhang, W., Munkholm, L.J., Liu, X., An, T., Xu, Y., Ge, Z., Xie, N., Li, A., Dong, Y., Peng, C., Li, S., Wang, J., 2023. Soil aggregate microstructure and microbial community structure mediate soil organic carbon accumulation: Evidence from one-year field experiment. *Geoderma* 430, 116324. <https://doi.org/10.1016/j.geoderma.2023.116324>.
- Zhang, X., Gregory, A.S., Whalley, W.R., Coleman, K., Neal, A.L., Bacq-Labreuil, A., Mooney, S.J., Crawford, J.W., Soga, K., Illangasekare, T.H., 2021. Relationship between soil carbon sequestration and the ability of soil aggregates to transport dissolved oxygen. *Geoderma* 403. <https://doi.org/10.1016/j.geoderma.2021.115370>.